

Journal of
***Mechanics of
Materials and Structures***

**QUASI-STATIC PUNCH INDENTATION OF A
HONEYCOMB SANDWICH PLATE: EXPERIMENTS
AND MODELLING**

Dirk Mohr, Zhenyu Xue and Ashkan Vaziri

Volume 1, N° 3

March 2006

QUASI-STATIC PUNCH INDENTATION OF A HONEYCOMB SANDWICH PLATE: EXPERIMENTS AND MODELLING

DIRK MOHR, ZHENYU XUE AND ASHKAN VAZIRI

Punching experiments on wide honeycomb sandwich beams were performed to evaluate the predictive capabilities of a newly developed constitutive model in structural applications. The employed constitutive model for plastically compressible orthotropic materials accounts for both non-uniform hardening and softening associated with stressing in different directions. This feature is vital when assessing the structural performance of metal sandwich plates with low density cellular cores. Pure shear and uniaxial compression tests have been carried out to identify the input stress-strain data for the constitutive model. The sandwich beam has been modeled with shell/beam elements for the face sheets and only one continuum element through-the-thickness for the honeycomb core material. Comparison of the numerical results with experimental observations validates the capability of the proposed approach based on continuum modeling of the core in capturing the main features of sandwich beam response under punch loading.

1. Introduction

Metallic sandwich structures have been used for decades in lightweight aerospace vehicles due to their high flexural stiffness-to-weight ratio. More recently, sandwich constructions are also considered in naval architecture. The general idea is to enhance the structural performance of ships under high intensity pressure loading through the use of outer hulls made in sandwich construction. [Hutchinson and Xue \[2005\]](#) have demonstrated that optimized all-metal sandwich plates may have distinct structural advantages over comparable weight monolithic plates under high intensity pulse. The virtual design of large-scale sandwich structures requires reliable computational models capable of predicting the mechanical response of sandwich structures for a wide spectrum of loading scenarios and geometries. The core layer of all-metal sandwich structures may consist of either random or periodic shell, plate and beam assemblies. Prominent examples are metallic foams,

Keywords: sandwich structures, finite element modeling, constitutive modeling, metallic honeycomb, plasticity.

honeycombs and truss lattice structures [Gibson and Ashby 1997]. Using state-of-the-art finite element software, the exact geometry of both the core layer and the face sheets may be modeled in detail and estimates of the overall structural behavior may be obtained with great accuracy [Mohr and Doyoyo 2004a; Xue and Hutchinson 2004a; Vaziri et al. 2006]. However, it is recognized that the computational costs associated with detailed models comprised of millions of finite elements are too high for use in an industrial environment. As an alternative to detailed modeling, various researchers have dealt with the development of constitutive models which describe the so-called macroscopic behavior of the sandwich core layer [Deshpande and Fleck 2000; Mohr and Doyoyo 2004c; Xue and Hutchinson 2004b; Rabczuk et al. 2004; Xue et al. 2005; Mohr 2005; Zok et al. 2005]. In other words, the discrete core layer structure is considered as a homogenous solid which allows for its discretization with solid elements, thereby drastically reducing the computational costs of simulating the response of large scale sandwich structures.

We emphasize here that this macroscopic modeling approach is of great value for practical engineers, even though it may not be satisfactory from a mathematical point of view. With respect to rigorous homogenization (for example, [Ponte Castañeda and Suquet 1998]), there are two important conditions which are frequently violated when developing macroscopic constitutive models for sandwich core materials. First, the condition of separation of length scales is seldom satisfied. This may lead to scale effects due to the dominance of boundary effects. Furthermore, the constitutive model predictions will be poor under the presence of large macroscopic stress and strain gradients. Second, the deformation in conventional sandwich core materials usually localizes at the macroscopic length scale when subject to compression (crushing), which rules out the applicability of established homogenization procedures.

The aim of this work is to assess the accuracy of a newly developed macroscopic model [Xue et al. 2005] in predicting the response of a wide honeycomb sandwich beam subject to punch loading. The model by Xue et al. [2005] invokes an ellipsoidal anisotropic yield surface in the six-dimensional stress space, an associated flow rule and a fully-coupled differential hardening/softening model. This specific model has been chosen since it can also account for strain-rate dependency, an important feature which is expected to become relevant in future studies on the blast resistance of sandwich structures. Here, we will evaluate the model performance for quasi-static loading. The experimental results of Mohr and Doyoyo [2004b], Wang and McDowell [2005] and Hong et al. [2006] have shown that the initial out-of-plane yield surface of honeycombs is of elliptical shape (Figure 1). This important feature has been incorporated into the constitutive model of Xue et al. [2005], thereby improving the poor performance of frequently used heuristic constitutive

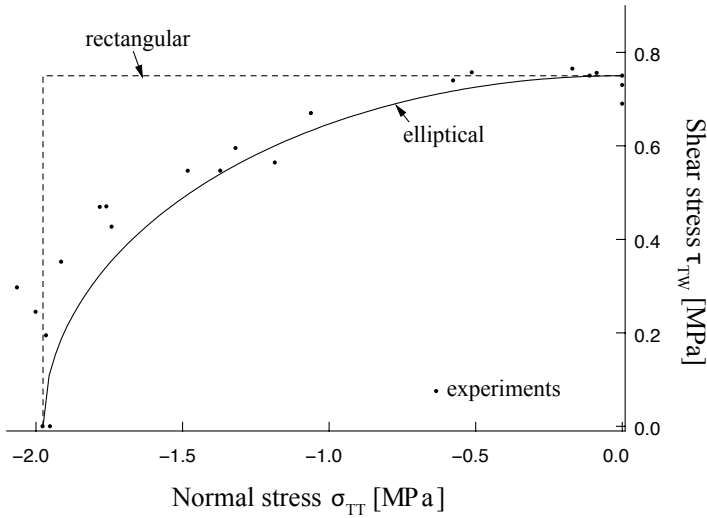


Figure 1. Initial yield surface of a metallic honeycomb core under combined compression and out-of-plane shear (σ_{TT}, τ_{TW}). The open dots represent experimental data points [Mohr and Doyoyo 2004b]. The solid line corresponds to the prediction from the ellipsoidal surface invoked in the present constitutive model of [Xue et al. 2005] when all the plastic Poisson ratios are zero. The dashed curve presents the ‘rectangular yield surface’ of the heuristic honeycomb models in LS-DYNA [LSTC 2000] and PamCrash [ESI 1999].

models for honeycombs [LSTC 2000; ESI 1999]. Observe from Figure 1 that the elliptical yield surface closely follows the experimental points while simple uncoupled models cannot represent the interaction of shear and normal stresses.

In this work, wide sandwich beams with hexagonal aluminum honeycomb core have been manufactured and subjected to punch loading. A newly developed two-actuator system is used to perform pure shear tests on a 1.8% relative density aluminum honeycomb in order to identify the associated input stress-strain data. Subsequently, the constitutive model of Xue et al. [2005] is calibrated and used to simulate the punch tests. From the comparison of experiments and simulations, we find that this computationally-efficient macroscopic model provides accurate predictions of the overall response for a rather complex loading scenario which includes both local and global deformation.

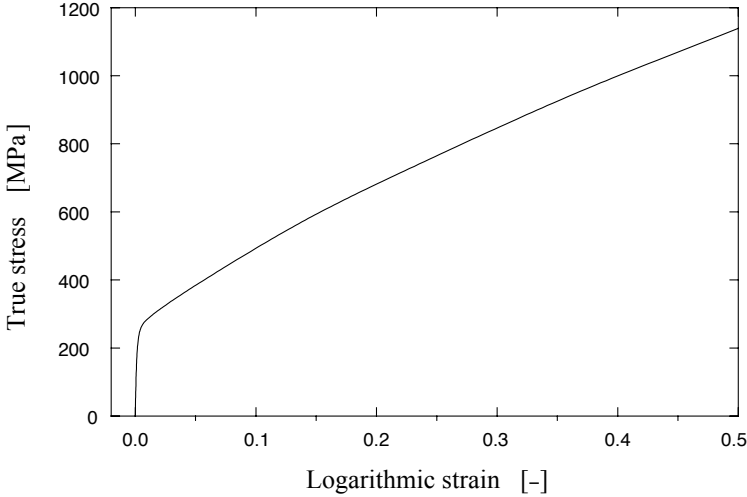


Figure 2. True stress versus logarithmic strain curve for the stainless steel 304 face sheets as obtained from uniaxial tensile testing of flat dogbone specimens.

2. Material

A custom-made sandwich material is used in this study. It is composed of an aluminum honeycomb core which is adhesively bonded to stainless steel face sheets. This lightweight core layer is $C = 15.9$ mm thick and contributes about 20% to the mass of the sandwich cross-section. The face sheets on the other hand have the thickness of $t_f = 0.2$ mm, which makes up for the remaining 80% of the cross-sectional mass. The weight contribution of the 0.1 mm thick adhesive layers (Lord 310A/B, Lord Corporation, Cary, NC) may be neglected.

2.1. Mechanical properties of the face sheets. The mechanical behavior of the stainless steel face sheets (Type 304, AlvestaPolarit, Sweden) has been determined from standard uniaxial tensile tests on dogbone-shaped specimens. The measured stress-strain curve, in terms of true stresses and logarithmic plastic strains, is shown in Figure 2. The face sheet material has the Young's modulus of $E = 200$ GPa and the initial yield strength of about $\sigma_f = 250$ MPa; it exhibits a pronounced strain hardening before the specimens fail at a strain of about $\varepsilon_f = 0.5$.

2.2. Honeycomb core. The honeycomb core material manufactured by Hexcel (Dublin, CA) is made from $t = 34\mu\text{m}$ thick aluminum 5056 foil; the single- and double-thickness cell walls of the hexagonal cells are respectively about $l = 3.1$ mm

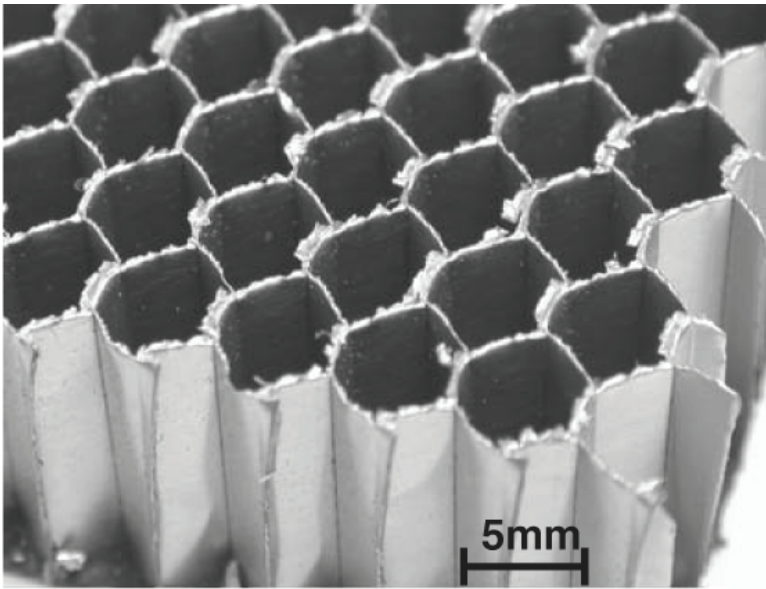
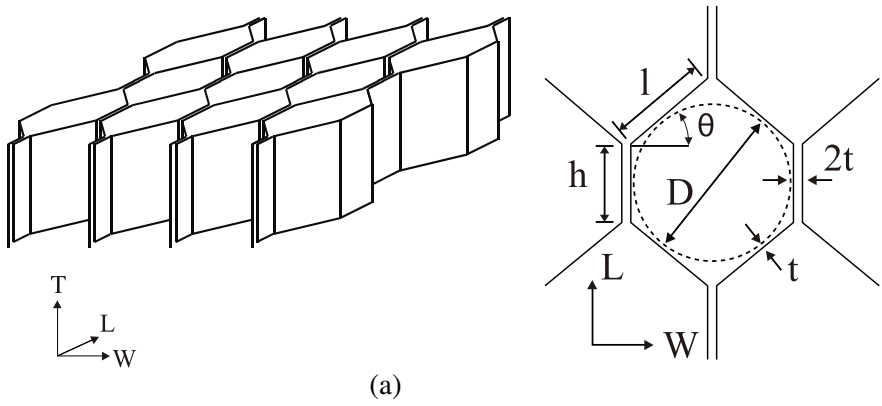


Figure 3. (a) Schematic of the hexagonal honeycomb core geometry; (b) photograph of the 1.8% relative density aluminum honeycomb.

in-plane			out-of-plane		
E_{WW}	E_{LL}	G_{WL}	E_{TT}	G_{TW}	G_{TL}
[MPa]	[MPa]	[MPa]	[MPa]	[MPa]	[MPa]
0.11	0.27	0.02	1252.76	155.77	315.19

Table 1. Elastic constants of the 1.8% relative density hexagonal honeycomb.

and $h = 2.4$ mm wide (Figure 3). The relative core density ρ^* of the honeycomb core can be obtained from

$$\rho^* = \frac{1 + \frac{h}{t}}{\cos \theta (\sin \theta + \frac{h}{t})}, \quad (1)$$

where θ is the cell wall opening angle, Figure 3 (a). This leads to the core density of $\rho^* \cong 1.8\%$ for the honeycomb core material study ($\theta = 40^\circ$). Table 1 summarizes the corresponding elastic constants of the honeycomb core. These have been evaluated from the classical formulas summarized in the textbook by Gibson and Ashby [1997] for a base material of $E_s = 72$ GPa. We note that the core material is highly orthotropic with a very small stiffness and strength in the WL -plane, where W and L denote the so-called in-plane directions of the honeycomb microstructure as shown in Figure 3. Conversely, the material is strong in the T -direction. Figure 4 shows a representative macroscopic stress-strain curve as obtained from uniaxial compression tests in the T -direction [Mohr and Doyoyo 2004b]. It is a well known characteristic of metallic honeycombs that the response curve for out-of-plane loading exhibits an initial peak stress which is significantly higher than the stress level in the so-called crushing regime. Densification starts at a logarithmic strain of about $\varepsilon_{TT}^d \cong -1.0$. In addition to the uniaxial compression tests, we designed a new experiment to determine the material response under pure shear loading in the WT -plane, which will be described in the following section.

3. Pure shear experiments

Sandwich structures are designed such that face sheets carry the bending and in-plane loads. The core layer on the other hand must sustain the shear loads. The shear lap test proposed in ASTM C273 may be suitable to determine the elastic shear modulus and the strength of brittle honeycombs, but it yields inconclusive results in the large deformation regime of low-density metallic honeycombs. This is due to the localization of deformation within the honeycomb microstructure which may cause the rotation of the grip plates. Consequently, the macroscopic strain field becomes non-uniform as well. Doyoyo and Mohr [2003] proposed a modified Arcan apparatus to overcome this problem, but their equipment has been limited to

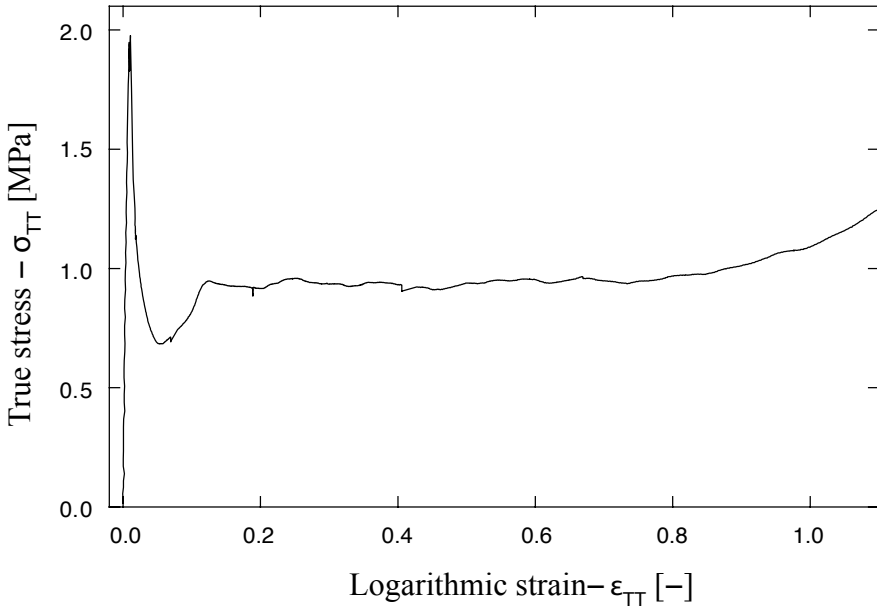


Figure 4. Experimental true stress-logarithmic strain relationships for the hexagonal aluminum honeycomb core under uniaxial compression along the T -direction.

relatively small butterfly specimens. Here, we make use of a hydraulic two-actuator system (custom made by Instron, Canton, MA) to characterize the macroscopic stress-strain curve for pure shear loading in the TW -plane. (Here, the term ‘pure shear’ is used to emphasize that the stress state is free from normal stresses which would be present in the case of ‘simple shear’.)

3.1. Experimental procedure. Figures 5 (a) and 5 (b) display a schematic and a photograph of the experimental setup, respectively. The specimen (part 8 as labeled in Figure 5 (b)) is composed of a 17 mm thick honeycomb core layer sandwiched between two 8 mm thick aluminum plates. A relatively thick adhesive layer is applied which imposes locally clamped boundary conditions on the honeycomb cell walls. This sandwich specimen is clamped between two nonrotating grip plates (parts 6 and 7). The top grip plate (part 7) is rigidly connected to the vertical actuator (part 1), which can only move along the vertical direction. The bottom grip plate (part 6) is attached to the horizontal actuator system (part 4). The same grip is mounted on a low friction slide table (part 5), which allows for the horizontal motion while preventing rotations. Since the rotation of both the top and the bottom

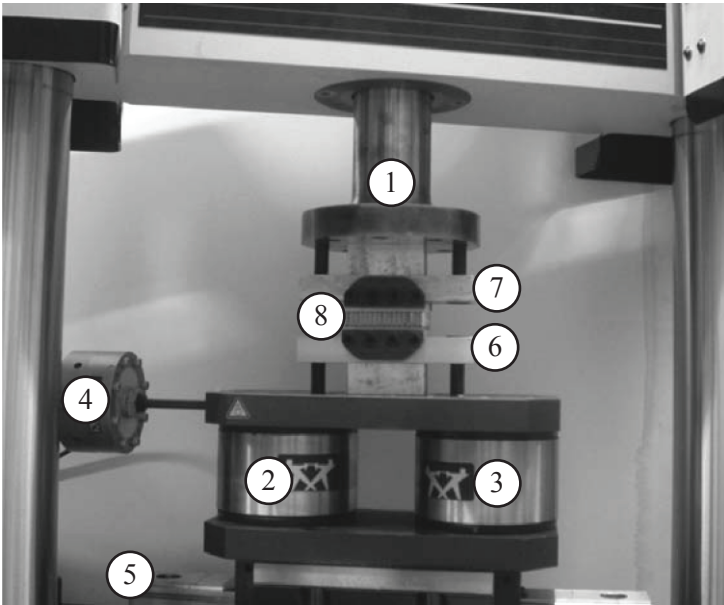
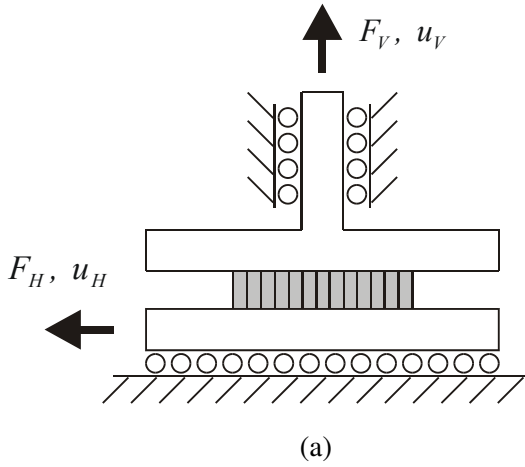


Figure 5. The experimental setup used for pure shear testing. (a) Schematic of the mechanical system. (b) Photograph of the biaxial testing system: (1) piston of the vertical actuator; (2) and (3) vertical load cells; (4) horizontal piston with load cell; (5) low friction slide table; (6) bottom grip plate; (7) top grip plate; (8) specimen.

grips are suppressed by the system, a bending moment builds up when a horizontal force is applied to the specimen. Thus, two parallel uniaxial load cells (parts 2 and 3) are used to measure the vertical force.

The experiments are performed in a combined load- and displacement-controlled mode. Unlike the simple shear test in which the vertical displacement must be kept constant ($u_V = 0$), the pure shear experiments must be performed under force control in order to keep the vertical force zero, that is, $F_V = 0$ while $u_V \neq 0$ (Figure 5 (a)). Using the hydraulic system control software (Fast Track, Instron, Canton, MA), the sum of the two vertical force measurements is defined as single virtual channel and consequently used to control the vertical actuator such that $F_V = 0$. The horizontal actuator has been controlled by the built-in LVDT for the horizontal position measurement.

The sandwich specimens are $l = 80\text{mm}$ long (along the W -direction) and $C = 17\text{mm}$ thick (in the T -direction) which corresponds to a length-to-thickness ratio of about 4.7. The specimen width in the L -direction is $w = 50\text{mm}$. Based on measurements of the horizontal force and the horizontal and vertical displacements, we define the engineering shear stress as

$$S_{TW} = \frac{F_H}{wl}, \quad (2)$$

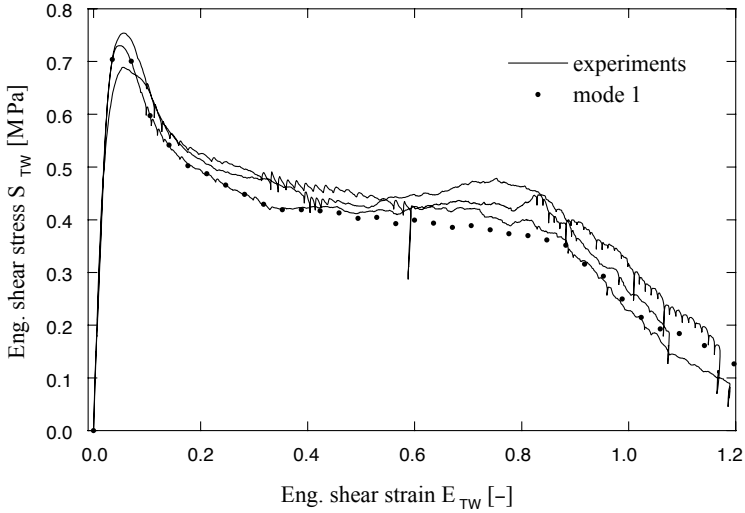
and the engineering shear and normal strains as

$$E_{TW} = \frac{u_H}{C} \quad \text{and} \quad E_{TT} = \frac{u_V}{C}, \quad (3)$$

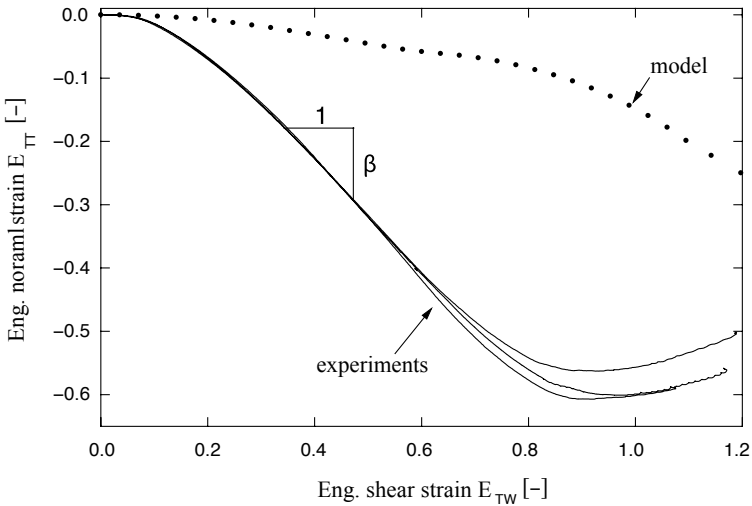
respectively. All tests have been carried out at a constant horizontal velocity of 3 mm/min.

3.2. The core response to pure shear loading. The measured shear stress versus shear strain curves are shown in Figure 6 (a). Selected photographs taken throughout the experiment are depicted in Figure 7. The material response is linear up to a shear stress of about 0.5 MPa. Beyond this point, the slope of this curve decreases slightly as shear buckles become visible within the honeycomb microstructure (Figure 7 (b)). The shear stress-strain curve reaches its maximum at about $\tau_{max} = 0.7\text{MPa}$ (point of shear failure) before it approaches a considerably lower plateau stress level of about 0.45 MPa. The stress level drops further as the honeycomb cell walls fracture at a shear strain of about 0.9. It is noteworthy that the high frequency fluctuations in the stress-strain curve are due to the immediate response of the two-actuator control system as macroscopic softening occurs throughout the combined vertical force/ horizontal displacement controlled experiments.

Both the photographs and the plot of the normal strain history (Figure 6 (b)) show the shear-induced compaction of the honeycomb material. In order to meet



(a)



(b)

Figure 6. Experiments and model calibration for pure shear: (a) engineering stress-strain curve; (b) shear-induced compaction. The model assumptions of associated plastic flow and zero plastic Poisson ratios are suitable for predicting the behavior at small strains, whereas nonassociated flow dominates for large shear strains.

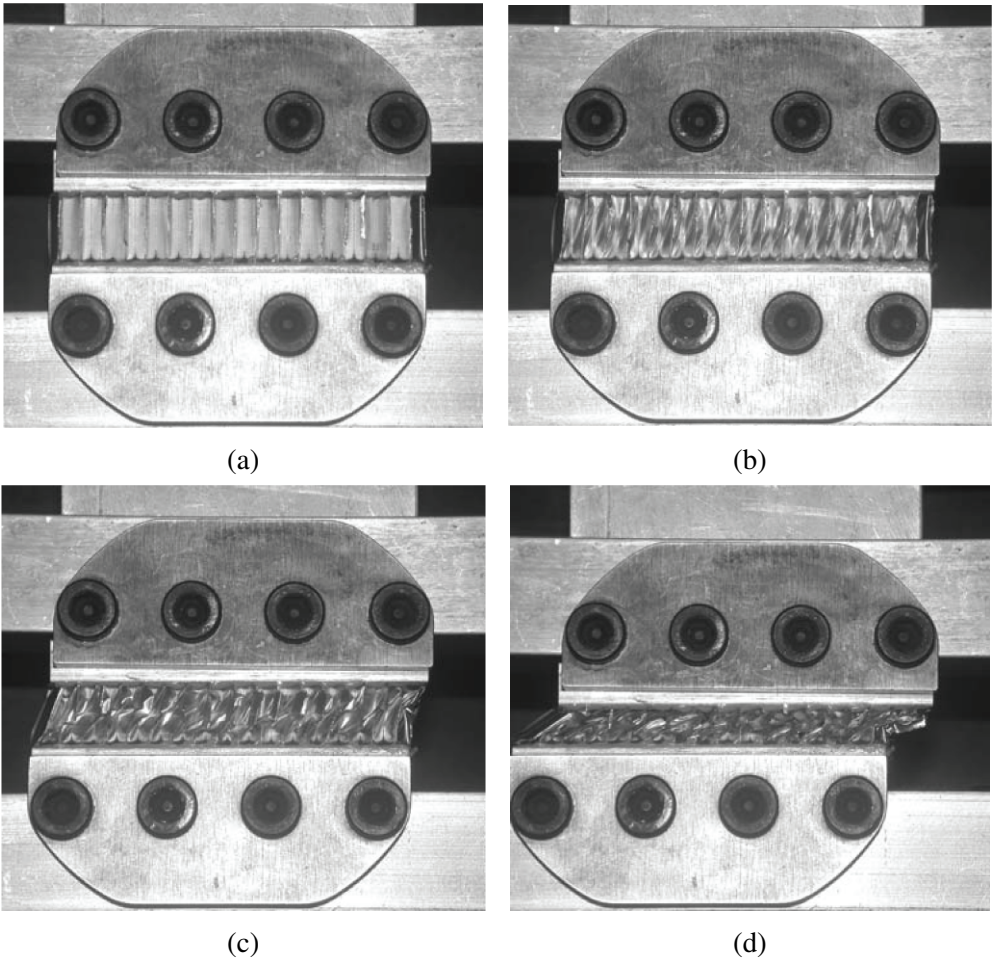
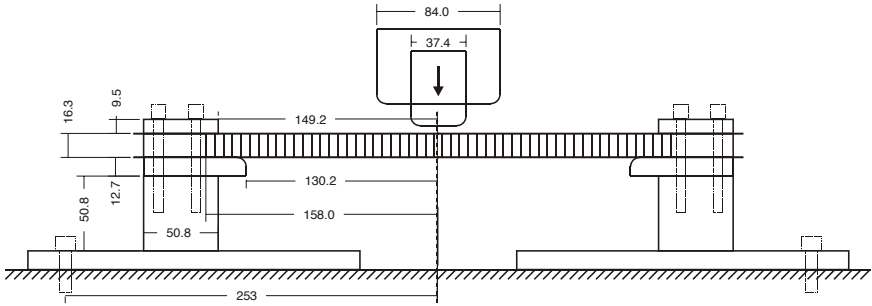


Figure 7. Deformed configuration of the honeycomb core specimen throughout pure shear testing at various stages of deformation: (a) $E_{TW} = 0$, (b) $E_{TW} = 0.04$, (c) $E_{TW} = 0.21$, and (d) $E_{TW} = 0.58$.

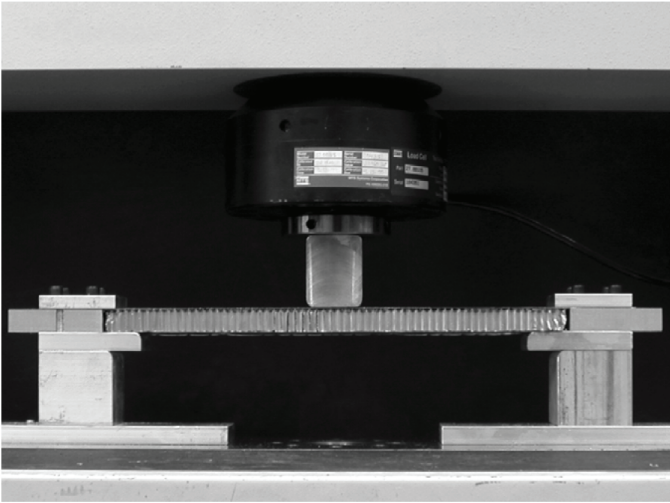
the pure shear condition of $F_V = 0$, the sandwich specimen reduces its thickness, that is, the strain increment is $dE_{TT} < 0$. The shear-induced normal strains are very small for shear strains below 0.1. However, for shear strains above 0.1, the deformation in the T -direction becomes considerable. For large shear strains, the shear compaction factor is approximately constant,

$$\frac{dE_{TT}}{dE_{TW}} \cong -\beta, \quad (4)$$

where $\beta = 0.88$ for the current experiment (Figure 6 (b)).



(a)



(b)

Figure 8. (a) Schematic of the experimental setup of the punch test. All dimensions are given in mm. (b) Photograph of the fixture with the custom made honeycomb sandwich beam. The width of all tested sandwich beams was $W=45.7$ mm.

4. Punching experiments

4.1. Experimental setup. Figure 8 shows a photograph and schematic of the experimental setup. A special fixture has been designed to clamp the $W = 45.7$ mm wide sandwich beams. The maximum unsupported length of the sandwich beam is $L = 260.4$ mm. The 15.9 mm thick sandwich core of the 16.3 mm thick sandwich plate has been replaced by equally thick aluminum blocks in the clamping

area. Four M6-12.8 cap screws are used at each end of the specimen to apply the clamping pressure to the 9.5 mm thick aluminum plates (Figure 8 (a)). The entire fixture is mounted on the base table of a screw-driven universal testing machine. Two punches of different sizes are used: a small punch of width 37.4 mm (Figure 8) and a large punch of 84 mm width. All corner radii of the punch and fixture are 6.35 mm. The punches are connected to a 200kN load cell which measures the vertical reaction force, P , exerted to the punch. Since the sandwich beam structure is considerably more compliant than the testing frame and fixture, we assume that the cross-head and punch displacement, u_p , are identical. The experiments are carried out at constant cross-head velocity of 5 mm/min.

4.2. The sandwich response to quasistatic punch indentation. A series of photographs is shown in the left column of Figures 9 and 10 for the small and large punch experiments, respectively. The measured force-displacement curves are shown by solid lines in Figure 11 (a). Figure 11 (b) shows the same curves again with an abscissa axis shift of 10 mm for punch displacements smaller than the sandwich beam thickness, $u_p \leq 16.3$ mm. Both force-displacement curves exhibit a peak at about $P_s \cong 1150$ N followed by a drop of about 200 N. Subsequently, the force-displacement curve increases in a nonlinear manner before it becomes approximately linear for punch displacements that are considerably larger than the sandwich beam thickness. In this regime, face sheet stretching dominates the response of the sandwich beam; the force-displacement curve for the small punch has a slope of 132 N/mm, whereas the slope of the large punch curve is about 157 N/mm. It may be seen from the photographs taken at a cross-head position of about 3 mm (Figures 9 (a) and 10 (a)) that the initial nonlinear response of the sandwich beam is dominated by the shear deformation of the core material. As for the pure shear tests (Figure 7), shear buckles become visible in the honeycomb cell walls of the unsupported beam cross-section. It appears that the initial peak of the force-displacement curve is due to the shear failure of the core material. Recall that the shear stress-strain curves exhibited a similar peak. This argument may be supported by the observation that this peak is approximately the same irrespective of the punch width. Denoting the maximum shear resistance of the core material by τ_{max} , the punch force P_s associated with the initial shear failure of the sandwich beam can be obtained using a simple beam analysis:

$$P_s = 2\tau_{max}CW. \quad (5)$$

According to the pure shear tests, we have

$$\tau_{max} = 0.75 \text{ MPa},$$

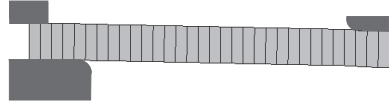
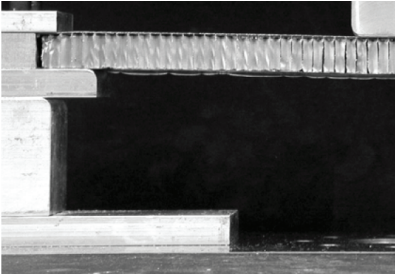
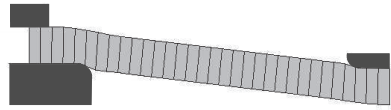
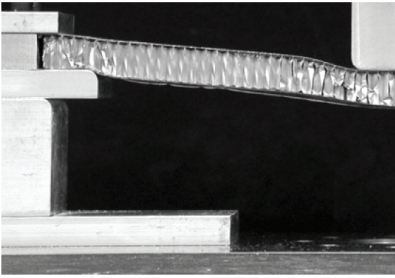
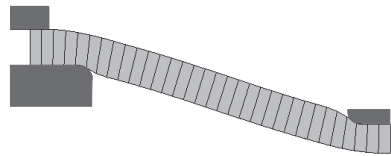
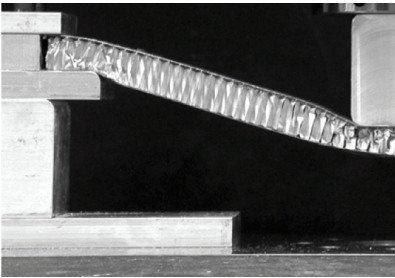
(a) $u_P = 3.1$ mm(b) $u_P = 17.5$ mm(c) $u_P = 41.5$ mm

Figure 9. Comparison of the experiments and simulations for the small punch (width=37.4 mm). The left column shows the photographs taken throughout the experiment and the right column depicts the corresponding deformed configurations of the sandwich beams as predicted from simulations.

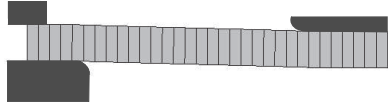
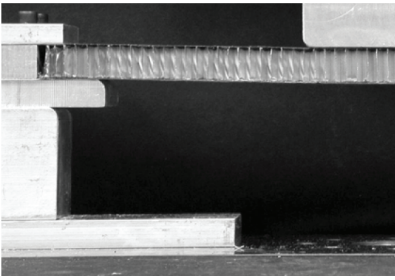
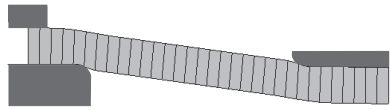
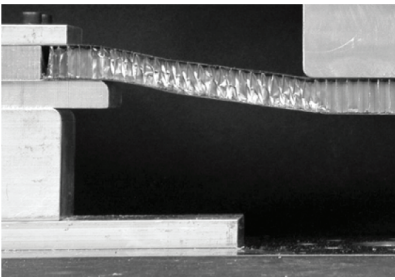
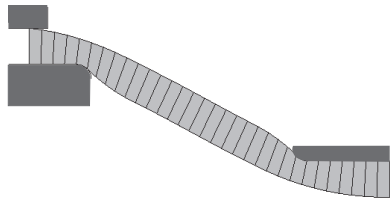
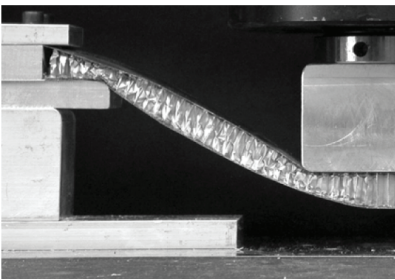
(a) $u_P = 2.8$ mm(b) $u_P = 16.5$ mm(c) $u_P = 58.5$ mm

Figure 10. Comparison of the experiments and simulations for the large punch. The left column show the photographs taken throughout experiments while the right column depicts the corresponding configurations as predicted from simulations.

resulting in $P_s = 1090$ N, which is in a good agreement with our experimental observations. After the shear failure of the core material, the small punch locally indents the sandwich beam (Figure 9 (b)). Local indentation is also observed in the vicinity of the clamped beam boundary. The pressure under the wide punch is smaller and it can be seen from Figure 10 (b) that the core material underneath the punch remains intact for displacements smaller than 16.5 mm. For large deflections, the shear deformation of the core material increases only slightly. Instead, both the top and bottom face sheets are substantially stretched which leads to a stiffening response. Since the distance between the punch and the support is smaller for the wide punch, the stretching of the face sheet is more intense for the same punch displacement, which explains the larger slope of the large punch force-displacement curve at large deflections.

5. Modeling

5.1. Constitutive modeling of the honeycomb core layer. A special version of the constitutive model proposed by Xue et al. [2005] for plastically compressible orthotropic materials is employed in this study to represent the core layer. Denoting the six independent components of the Cauchy stress tensor by the vector

$$\boldsymbol{\sigma} = (\sigma_1, \sigma_2, \sigma_3, \sigma_4, \sigma_5, \sigma_6)^T \equiv (\sigma_{TT}, \sigma_{WW}, \sigma_{LL}, \sigma_{TL}, \sigma_{WL}, \sigma_{TW})^T$$

(where the initial coordinate frame is aligned with the orthotropy axes of the honeycomb core), the characteristic ellipsoidal yield surface is written in the form

$$f(\boldsymbol{\sigma}, \mathbf{s}) = \sum_{i=1}^6 \left(\frac{\sigma_i}{s_i} \right)^2 - 1 = 0, \quad (6)$$

where \mathbf{s} denotes the corresponding vector of deformation resistances. (In the proposed constitutive model, an ellipsoidal yield surface is invoked that generalizes Hill's surface for orthotropic plastically incompressible materials. The general formulation of this constitutive model is able to incorporate nonconstant plastic Poisson ratios in the axes of anisotropy—that is, the plastic Poisson ratios can be a function of plastic strains. However, for the current study the plastic deformation of the core is approximated by taking all plastic Poisson ratios as zero.) Within the framework of associated incremental plasticity, strain hardening/softening is taken into account by the evolution of the deformation resistance. More specifically, we take the independent hardening/softening approach where the evolution of individual components of the vector of deformation resistance, s_i , depends only on the corresponding true plastic strain components, ε_i^P , where

$$\boldsymbol{\varepsilon}^P = (\varepsilon_1^P, \varepsilon_2^P, \varepsilon_3^P, \varepsilon_4^P, \varepsilon_5^P, \varepsilon_6^P)^T \equiv (\varepsilon_{TT}^P, \varepsilon_{WW}^P, \varepsilon_{LL}^P, 2\varepsilon_{TL}^P, 2\varepsilon_{WL}^P, 2\varepsilon_{TW}^P)^T.$$

In other words, we have $s_i = s_i(\varepsilon_i^P)$.

In the present punching experiment, the core material is predominantly loaded in the TW -plane. Therefore, the strain hardening/softening functions for uniaxial loading along the T -axis, $s_{TT}(\varepsilon_{TT}^P)$, and for shear loading in the TW -plane, $s_{TW}(2\varepsilon_{TW}^P)$, must be calibrated with fidelity. The in-plane functions $s_{WW}(\varepsilon_{WW}^P)$ and $s_{LL}(\varepsilon_{LL}^P)$ are also important from a theoretical point of view, but due to the strong orthotropy of the hexagonal aluminum honeycomb, the contribution of the in-plane stresses to the overall response of the sandwich beam may be neglected. [Table 1](#) shows a summary of the elastic constants as evaluated for the 1.8% relative density hexagonal aluminum honeycomb. Recall that these have been estimated for all loading directions according to the analytical expressions given in the textbook by [Gibson and Ashby \[1997\]](#).

As far as the determination of $s_{TT}(\varepsilon_{TT}^P)$ and $s_{TW}(2\varepsilon_{TW}^P)$ is concerned, it is noteworthy that the cell walls of the aluminum honeycomb buckle elastically before yielding plastically. It is reasonable to assume that macroscopic yield initiates as the stress level reaches the characteristic initial peak of the stress-strain curves [[Mohr and Doyoyo 2004a](#)]. Upon evaluation of the experimental results, we obtain the initial yield stresses $s_{TT}(\varepsilon_{TT}^P = 0) = 1.95$ MPa and $s_{TW}(2\varepsilon_{TW}^P = 0) = 0.69$ MPa for crushing and shearing, respectively. The experimental curves from [Figures 4](#) and [6 \(a\)](#) have been converted into the functions $s_{TT}(\varepsilon_{TT}^P)$ and $s_{TW}(\varepsilon_{TW}^P)$ by assuming nonevolving elastic moduli, that is,

$$\varepsilon_{TT}^P = \varepsilon_{TT} - \frac{s_{TT}}{E_{TT}} \quad \text{and} \quad 2\varepsilon_{TW}^P \cong E_{TW} - \frac{s_{TW}}{G_{TW}}. \quad (7)$$

The approximation sign is used in the latter equation since it does not account for the rotation of the principal axes of the stretch tensor in the shear test. The validity of this approximation is examined by simulating the pure shear test using the constitutive model. The comparison of the solid and dotted curves in [Figure 6 \(a\)](#) confirms the validity of this simplification. Note from [Figure 6 \(b\)](#) that the shear-induced compaction of the core material may not be captured by the present model. The model response to uniaxial loading along the T -direction is identical to the experimental curve shown in [Figure 4](#).

5.2. Modeling of the wide sandwich beam. In the development of the macroscopic constitutive model, it is assumed by the definition of the macroscopic strains (see [Equation \(3\)](#)) that the displacement field is linear along the core thickness (T -direction). Therefore, the core is discretized using only one row of elements with linear shape functions along the thickness direction. Using a single linear element along the thickness implies the assumption that initially flat cross-sections remain flat throughout bending. However, it is important to note that commonly used numerical integration schemes may not be accurate enough to capture substantial

variations in the stress field along the thickness direction. Therefore, the present modeling approach is only recommended when the contribution of the core material to the overall bending resistance of the sandwich sheet is negligible.

In the case of sandwich structures with curved mid-planes, the element edges must be aligned with the thickness direction of the core layer. The number of elements along the sandwich mid-axis on the other hand shall be chosen such that the continuum boundary value problem is solved with satisfactory accuracy. In the constitutive model, the honeycomb core is considered as a so-called simple material body. The model calibration experiments are almost stress gradient free (for example, $\delta\sigma_{TT}/\delta X_W \cong 0$). However, from a physical point of view, it may be expected that large macroscopic stress gradients affect the material response due to the discreteness of the cellular core structure along W - and L -directions, which indicates the need for enriched Cosserat type of theories [Onck 2002]. Therefore, it is emphasized that the present model predictions may not be satisfactory in regions where the continuum solution indicates large gradients in either the stress or strain field.

Another consideration in modeling sandwich structures as a three layer shell-solid-shell assembly is the continuity of the displacement field which is enforced at the common nodes of the face sheets and the core layer. These nodes are positioned in the face sheet mid-plane whereas in reality, the displacement continuity is enforced at the contact surfaces between the core and face sheets. There are basically three modeling options: (1) using the exact core thickness while the face sheet separation in the model is smaller than in reality; (2) using the exact face sheet separation, while artificially increasing the core thickness; (3) programming a user-defined sandwich element with enhanced kinematics to take this effect into account. With respect to sandwich sheet failure, two key mechanical quantities depend directly on either the face sheet separation $C + t_f$ or the core height C : the overall plastic bending moment, M_{pl} , and the shear strength, F_s , may be respectively approximated as

$$M_{pl} = \sigma_f t_f (C + t_f) W \quad \text{and} \quad F_s = \tau_{max} C W. \quad (8)$$

Both quantities show a linear dependence which demonstrates that the error associated with the model assumptions (1) or (2) is small if $t_f/C \ll 1$. In the present problem, we have $t_f/C \cong 1\%$.

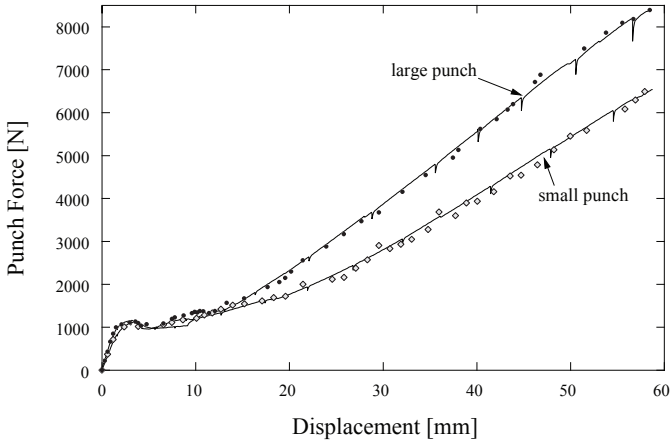
5.3. Modeling of the punching experiments. The punching of the wide beam is treated as a two-dimensional problem. We hypothesized that the deformation of the core material in the L -direction can be neglected. Consequently, four-node plane strain elements with reduced integration (element CPE4R in [Abaqus 2005]) are employed for the honeycomb core layer. The thin face sheets are discretized by a

two-node Timoshenko beam element (element B21 in [Abaqus 2005]). Each beam element has a rectangular cross section of height $t_f = 0.2$ mm and a unit width.

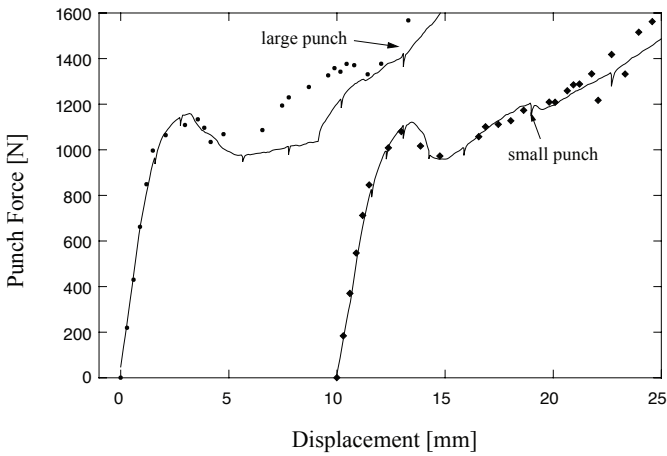
Only one half of the whole system is analyzed due to the symmetry of the structure and the loading conditions. Symmetry boundary conditions are applied to the center cross section of the wide beam. The horizontal displacements of all nodes along each edge of the sandwich beam are restricted to be zero. The punch and all support structures are modeled by rigid elements with frictionless contact between each pair of contact surfaces. The support structures are fixed, while the punch loads is applied at a constant vertical velocity. The calculations are performed using ABAQUS/explicit. In comparison with the standard implicit algorithm, the explicit scheme is chosen due to its advantages in handling sliding contact conditions and the overall softening behavior of the honeycomb core due to the presence of stabilizing inertia. Oscillations due to this dynamic stabilization have been found to be negligibly small as compared to the static force level.

Note that the propagation velocities of uniaxial waves in the sandwich material are about 5000 m/s for both longitudinal waves along the face sheets and waves through the thickness of the honeycomb material. In order to ensure quasistatic loading conditions, the characteristic durations for elastic waves traveling from the punch center to the clamping support of the sandwich plate (about $30 \mu\text{s}$) and through the thickness of the sandwich sheet (about $3 \mu\text{s}$) must be several orders of magnitudes smaller than the total duration of the punching simulations. Here, the numerical simulations are carried out for a constant punch velocity of 1 mm/s, which corresponds to a total duration of 60 s. Regarding the computational efficiency of the simulations, it is worth noting that the stable time step is mostly governed by the wave propagation in the face sheets. Stability of the explicit time integration scheme requires the time step to be smaller than the duration of a wave propagating between two opposite sides of the element, that is, $\Delta t < l_e/c$ (in a nonrigorous sense), where l_e and c denote the characteristic element side length and wave speed, respectively. According to the continuum model of the core, the in-plane wave propagation speed in the present honeycomb core is extremely small (about 100 times slower than the out-of-plane wave). Thus, if the sandwich core height is larger than the element length along the sandwich mid-axis, the elements of the face sheets will control the critical time step.

5.4. Comparison of the results from experiments and simulations. The punching simulations are carried out for three different mesh densities along the sandwich mid-axis by employing 32, 64 and 128 elements along the sandwich mid-axis. No remarkable difference is observed between the force-displacement curves obtained using the three mesh densities. Even coarser meshes may be suitable for modeling the sandwich sheet, but the contact algorithm is likely to fail when the model no



(a)



(b)

Figure 11. Comparison of the experimental results of the honeycomb core sandwich beam subject to quasistatic punch indentation (solid line) with the predictions from the numerical simulations based on the continuum modeling of the core. (a) Punch force-displacement curve for displacements of up to 60 mm; (b) detail of that curve for small displacements ($u_P \leq C = 16.3$ mm). The origin of the curve for the small punch has been shifted by 10 mm.

longer captures important details of the face sheet deformation near the rigid punch and support structures. The direct comparison of the experimental and computational force-displacement curves is shown in [Figure 11 \(a\)](#). The experimental and numerical curves are considerably close for small and large displacements. Both the initial slope in the elastic regime and the following peak load are accurately predicted by the numerical model ([Figure 11 \(b\)](#)). Similarly, excellent agreement is observed for large displacements, where the sandwich response is mostly governed by the stretching of the face sheets.

In order to compare the predicted displacement fields, we plotted the deformed *FE*-meshes next to selected photographs taken during the experiments at the same vertical displacements. Again, we observe good overall agreement of experiments and simulations. In particular, the development of two separate regions of shear-dominated and compression-dominated core deformation seems to be captured in close analogy with the experiment.

6. Discussion

The main result of this study is that this rather simple computational model can predict the response of a wide sandwich subject to punch loading with considerable fidelity. Due to the high orthotropy of the core material and the strength disparity between the core and face sheets, the sandwich core layer could be successfully modeled with only one element over the thickness. It is important to calibrate the plastic part of the core constitutive model from both uniaxial and pure shear test data. Recall that the punch force-displacement curve is governed by the shear behavior of the core material at the early stage of deformation.

Recent findings in cellular plasticity indicate that modeling of the fold propagation in honeycombs may require enriched constitutive theories [[Mohr and Doyoyo 2003](#)]. At the microscale, the through-the-thickness response of honeycomb sandwich sheets is characterized by the localization of deformation which may result in mesh dependency. This challenge has been successfully overcome by the present modeling approach through the use of only one element through the core thickness. This approach is suitable in sandwich applications when the stress and strain gradients along the in-plane directions are small. In the present study, this requirement is violated near the corners of the punch, but the comparison of experiments and simulations reveals that such local violations are still acceptable in a larger system. Another important outcome of preceding experimental studies on aluminum honeycombs is the observation of nonassociated plastic flow at large strains [[Mohr and Doyoyo 2004c](#); [Hong et al. 2006](#)]. The present model assumes associated plastic flow which appears to be a suitable assumption for small deformations ([Figure 6\(b\)](#)). Initially, the measured normal strains are almost zero,

which corresponds to associated flow with respect to the ellipsoidal yield surface, while for large shear strains substantial normal strain arises as described by the finite-strain constitutive model of [Mohr and Doyoyo \[2004c\]](#). In the present experiments, the shear strains do not exceed 0.2, which explains the applicability of the present model. Furthermore, there is no difference between the nonassociated and associated flow models for uniaxial compression within the large deformation zone directly underneath the punch.

7. Conclusion

A detailed study has been performed to evaluate the predictive capabilities of a newly developed constitutive model for sandwich core materials [[Xue et al. 2005](#)]. A new pure shear test for cellular solids has been presented and used to obtain the material model parameters for a thin-walled hexagonal aluminum honeycomb. All-metal sandwich beams have been constructed by bonding a 16 mm thick slice of this honeycomb to a pair of 0.2 mm thick stainless steel face sheets. Using a special clamping fixture, these wide sandwich beams have been loaded under quasistatic loading conditions with punches of different widths. The response of sandwich beams to punch loading has been analyzed in detail and predicted from finite element simulations by employing a continuum constitutive model for the sandwich core. The computational model exploits a single linear solid element for the core material in conjunction with two beam elements for the face sheets, which leads to a significant reduction of the computational time as compared to detailed modeling of the cellular core structure. The comparison of the numerical and experimental results demonstrates the good predictive capabilities of this simple computational model for studying the structural performance of metal sandwich beams.

Acknowledgments

The authors would like to thank Professors T. Wierzbicki and J.W. Hutchinson for valuable discussions. Mark Shorey from Instron (Canton, MA) is thanked for his help in designing the two-actuator testing machine. Financial support through ONR grants N00014-02-01-0700 and GG10376-114934 is gratefully acknowledged.

References

- [Abaqus 2005] Abaqus, *Abaqus version 6.5 reference manuals*, Providence, R.I: Abaqus Inc., 2005.
- [Deshpande and Fleck 2000] V. S. Deshpande and N. A. Fleck, “[Isotropic constitutive models for metallic foams](#)”, *J. Mech. Phys. Solids* **48**:6-7 (2000), 1253–1283.
- [Doyoyo and Mohr 2003] M. Doyoyo and D. Mohr, “[Microstructural response of aluminum honeycomb to combined out-of-plane loading](#)”, *Mech. Mater.* **35**:9 (2003), 865–876.

- [ESI 1999] ESI, *PamCrash reference manuals*, France: Engineering Systems International, 1999.
- [Gibson and Ashby 1997] L. J. Gibson and M. F. Ashby, *Cellular solids: structure and properties*, 2nd ed., Cambridge University Press, Cambridge, 1997.
- [Hong et al. 2006] S.-T. Hong, J. Pan, T. Tyan, and P. Prasad, “Quasi-static crush behavior of aluminum honeycomb specimens under compression dominant combined loads”, *Int. J. Plast.* **22**:1 (2006), 73–109.
- [Hutchinson and Xue 2005] J. W. Hutchinson and Z. Xue, “Metal sandwich plates optimized for pressure impulses”, *Int. J. Mech. Sci.* **47**:4-5 (2005), 545–569.
- [LSTC 2000] LSTC, *LS-DYNA reference manuals*, Livermore, CA: Livermore Software Technology Corporation, 2000.
- [Mohr 2005] D. Mohr, “Mechanism-based multi-surface plasticity model for ideal truss lattice materials”, *Int. J. Solids Struct.* **42**:11-12 (2005), 3235–3260.
- [Mohr and Doyoyo 2003] D. Mohr and M. Doyoyo, “Nucleation and propagation of plastic collapse bands in aluminum honeycomb”, *J. Appl. Phys.* **94**:4 (2003), 2262–2270.
- [Mohr and Doyoyo 2004a] D. Mohr and M. Doyoyo, “Deformation-induced folding systems in thin-walled monolithic hexagonal metallic honeycomb”, *Int. J. Solids Struct.* **41**:11-12 (2004), 3353–3377.
- [Mohr and Doyoyo 2004b] D. Mohr and M. Doyoyo, “Experimental investigation on the plasticity of hexagonal aluminum honeycomb under multiaxial loading”, *J. Appl. Mech. (Trans. ASME)* **71**:3 (2004), 375–385.
- [Mohr and Doyoyo 2004c] D. Mohr and M. Doyoyo, “Large plastic deformation of metallic honeycomb: orthotropic rate-independent constitutive model”, *Int. J. Solids Struct.* **41**:16–17 (2004), 4435–4456.
- [Onck 2002] P. Onck, “Cosserat modeling of cellular solids”, *C. R. Mécanique* **330**:11 (2002), 717–722.
- [Ponte Castañeda and Suquet 1998] P. Ponte Castañeda and P. Suquet, “Nonlinear composites”, *Adv. Appl. Mech.* **34** (1998), 171–302.
- [Rabczuk et al. 2004] T. Rabczuk, J. Y. Kim, E. Samaniego, and T. Belytschko, “Homogenization of sandwich structures”, *Int. J. Numer. Methods Eng.* **61**:7 (2004), 1009–1027.
- [Vaziri et al. 2006] A. Vaziri, Z. Xue, and J. W. Hutchinson, “Metal sandwich plates with polymer foam-filled cores”, *Journal of Mechanics of Materials and Structures* **1**:1 (2006), 97–127.
- [Wang and McDowell 2005] A. J. Wang and D. L. McDowell, “Yield surfaces of various periodic metal honeycombs at intermediate relative density”, *Int. J. Plast.* **21**:2 (2005), 285–320.
- [Xue and Hutchinson 2004a] Z. Xue and J. W. Hutchinson, “A comparative study of impulse-resistant metal sandwich plates”, *Int. J. Impact Eng.* **30**:10 (2004), 1283–1305.
- [Xue and Hutchinson 2004b] Z. Xue and J. W. Hutchinson, “Constitutive model for quasi-static deformation of metallic sandwich cores”, *Int. J. Numer. Methods Eng.* **61**:13 (2004), 2205–2238.
- [Xue et al. 2005] Z. Xue, A. Vaziri, and J. W. Hutchinson, “Non-uniform hardening constitutive model for compressible orthotropic materials with application to sandwich plate cores”, *Comput. Model. Eng. Sci.* **10**:1 (2005), 79–96.
- [Zok et al. 2005] F. W. Zok, H. Rathbun, M. He, E. Ferri, C. Mercer, R. M. McMeeking, and A. G. Evans, “Structural performance of metallic sandwich panels with square honeycomb cores”, *Philos. Mag.* **85**:26-27 (2005), 3207–3234.

DIRK MOHR: mohr@mit.edu

*Impact and Crashworthiness Laboratory, Massachusetts Institute of Technology, Cambridge, MA,
United States*

<http://web.mit.edu/mohr/www>

ZHENYU XUE: xue@deas.harvard.edu

*Division of Engineering and Applied Sciences, Harvard University, Cambridge, MA,
United States*

ASHKAN VAZIRI: avaziri@deas.harvard.edu

*Division of Engineering and Applied Sciences, Harvard University, Cambridge, MA,
United States*

www.deas.harvard.edu/~avaziri